Quantum cascade lasers monolithically integrated on germanium

K. Kinjalk, A. Gilbert, A. Remis, Z. Loghmari, L. Cerutti, G. Patriarche, M. Bahriz, Roland Teissier, A. Baranov, J. Rodriguez, et al.

Quantum cascade lasers monolithically integrated on germanium.

K. KINJALK[1]*, A. GILBERT[1], A. REMIS[1], Z. LOGHMARI,[1,2] L. CERUTTI[1], G. PATRIARCHE[3], M. BAHRIZ[1], R. TEISSIER,[1,2] A.N. BARANOV[1], J.-B. RODRIGUEZ[1] AND E. TOURNIE[1]

[1]*IES, University of Montpellier, CNRS, Montpellier, France*
[2]*Present address: MIRSENSE, Montpellier, France*
[3]*C2N, CNRS, Univ. Paris-Saclay, Palaiseau, France*
* *kumar.kinjalk@ies.univ-montp2.fr*

Abstract: Silicon (Si) photonics can have a major impact on the development of mid-IR photonics by leveraging on the reliable and high-volume fabrication technologies already developed for microelectronic integrated circuits. Germanium (Ge), already used in Si photonics, is a prime candidate to extend the operating wavelength of Group IV-based photonic integrated circuits beyond 8 µm, and potentially up to 15 µm. High performance quantum cascade lasers (QCLs) and interband cascade lasers grown on Si have been demonstrated, whereas no QCLs monolithically integrated on Ge have been reported yet. In this work, we present InAs-based QCLs directly grown on Ge by molecular beam epitaxy. The lasers emitting near 14 µm exhibited threshold current densities as low as 0.8-0.85 kA/cm^2 at room temperature.

1. Introduction

Mid-infrared (mid-IR) integrated photonics is expected to provide key advances for the demonstration of systems on chip. The main foreseen applications are free space optical communications and mid-IR spectroscopy sensing with portable and cost-effective systems. Different solutions are currently explored for the development of integrated mid-IR platforms, based on chalcogenide glasses thanks to their wide mid-IR transparency window [1], or III-V materials with direct integration of quantum cascade lasers (QCLs) [2] or interband cascade lasers [3]. Silicon (Si) photonics can have a major impact on the development of mid-IR photonics by leveraging the reliable and high-volume fabrication technologies already developed for microelectronic integrated circuits [4]. Interestingly, germanium (Ge), already used in Si photonics, is a prime candidate to extend the operating wavelength of Group IV-based photonic integrated circuits beyond 8 µm, and potentially up to 15 µm [5]. Furthermore, Ge benefits from a strong third-order nonlinearity which can also be advantageously exploited for the development of active devices [6]. In recent years, the development of a photonic platform based on Ge or Ge-rich SiGe alloys and dedicated to long mid-IR wavelengths has witnessed a burst of research activity [7], which encourages the integration of new devices, especially laser sources. Quantum dot lasers emitting at 1.3 µm grown on Ge have been reported [8]. In this work, we present long-wavelength InAs-based QCLs directly grown on Ge by molecular beam epitaxy (MBE).

2. QCL fabrication

Monolithic integration of III-V devices on Ge is concerned by the same problems as the direct growth of these materials on silicon. The device performances are strongly affected by the different crystal structures of the III-V compounds and group-IV semiconductors, which results

in the formation of anti-phase domains (APD) with opposite polarities within the III-V material [9]. The boundaries between these domains with inverted crystallographic orientation create parasitic current channels that shorten the active region of the devices [9]. Another issue is the large lattice mismatch between Ge and the materials used in mid-IR photonics which reaches 7% in the case of InAs- and GaSb-based structures. This mismatch is released through the generation of dislocations that can thread through the heterostructure and degrade the photonic devices grown on the mismatched substrate [8]. Our previous results showed however that InAs/AlSb QCLs grown on Si were not largely concerned by the above-mentioned problems. Performances of the devices emitting at 11 [2] and 7.5 µm [10] were similar to those of their counterparts grown on native InAs substrates. The first QCLs on Si were grown on substrates with a 6° cut, which favored a growth mode that provided domination of one of the crystallographic polarities [2]. The impact of the remaining threading dislocations was probably partially compensated for in these devices by the decreased interface roughness provided by the employed growth mechanism, resulting in a higher QCL gain. In the next work, an on-axis (001) Si substrate was used for growth which was initiated by a specially developed procedure aimed at annihilation of APDs in a buffer layer, preventing their penetration into the QCL active zone [10]. The density of the threading dislocations in these wafers grown on Si reached 10^8 cm^{-2} but the high performance of the fabricated lasers evidenced that the impact of dislocation-related defects on the device operation was quite weak. This finding is primarily due to the very short lifetimes of intersubband transitions, which makes them less sensitive to parasitic recombination channels compared with most of interband emitters. Also, the chemical composition of multicomponent III-V alloys grown on Si can be modified by mechanical strains in vicinity of the dislocations, affecting the band structure and consequently the operation of the concerned devices, such as GaInAs/AlInAs/InP QCLs [11]. In InAs/AlSb QCLs, the effect of this mechanism is negligible. Thus, the main problem in fabricating InAs-based QCLs on Ge is to provide an APD-free surface during the initial growth stage. The procedure employed for the growth on Si cannot be directly transferred to the growth on Ge because of the different chemical nature of these materials.

In this work, the QCL structures were grown by solid-source MBE on a (001) n-Ge substrate with a residual miscut of ~0.5°. Prior to the QCL growth, a template consisting of a 1.5-µm-thick nominally undoped p-GaSb buffer layer capped by a 100-nm-thick, nominally undoped, n-InAs layer was first grown using a specially developed procedure to promote burying of the

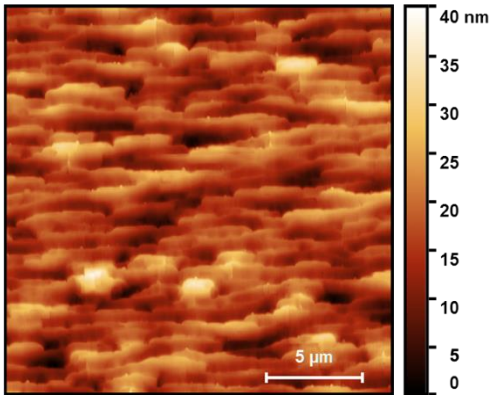

Fig.1. AFM image of the template.

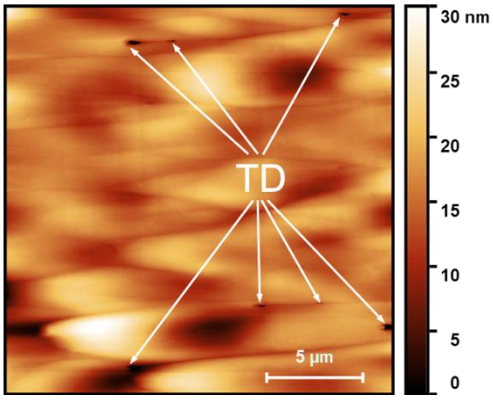

Fig.2. AFM image of the wafer EQ1092. A few threading dislocations (TD) are indicated.

APDs in the GaSb layer [12]. The template grown in a Riber C21 MBE system was then transferred to a Riber R412 machine for the growth of the QCL structure EQ1092. The growth in R412 was started by thermally desorbing the native oxide of the InAs layer at conditions usually used to deoxidize InAs substrates. The InAs and AlSb layers were grown at deposition

rates of 3.03 and 1A/s, respectively, and a V/III flux ratio of ~2. A reference QCL structure EQ1091 was previously grown on an InAs substrate. The active zone of the QCL consists of 45 repetitions of the following layer sequence, in Å and starting from the injection barrier: **26**/41/**1**/62/**1**/67/**2**/66/**2**/64/**6**/64/**6**/62/**6**/59/**9**/58/**10**/57/**11**/56, where AlSb layers are in bold and the Si-doped layers are underlined. The total electron sheet density N_s in the structure, taking into account the residual doping of InAs, is considered to be about 1×10^{11} cm^{-2} per period. The active zone is separated from 3-µm-thick InAs cladding layers doped with Si to 6×10^{17} cm^{-3} by 3-µm-thick undoped InAs spacers. The images of the template surface obtained by atomic

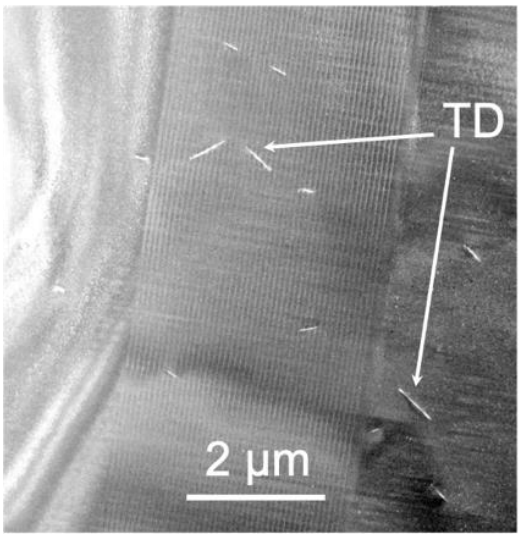

Fig.3. Cross-section TEM image of the QCL grown on Ge. Two threading dislocations (TD) are indicated.

force microscopy reveal the absence of APDs emerging at the template surface (Fig.1). The surface exhibit terraces with edges perpendicular to the direction of the substrate miscut. The rms roughness is 3.5 nm. After QCL growth, the surface is slightly undulated, with a rms roughness of 3.8 nm (Fig.2), a much better value than what we previously achieved on Si substrates [10]. The absence of APDs reaching the active zone has been confirmed by transmission electron microscopy (Fig. 3). In contrast, threading dislocations are clearly seen in both AFM and TEM images of the EQ1092 wafer (Fig.2 and 3, respectively). From this and other images, the density of dislocations threading the active zone is estimated to be in the low 10^7 cm^{-2}. Such a density, however, is at the limit of TEM resolution and we can only give a rough – albeit informative – estimate. As expected from the different lattice mismatch, this value is much lower than the ~10^8 cm^{-2} value obtained for QCLs grown on Si [10].

The overlap of the fundamental mode with the active region, Γ, and the waveguide loss for an empty waveguide, α_w, were calculated to be 0.5 and 3.6 cm^{-1}, respectively. The waveguide loss associated with light absorption by free carriers in the doped cladding layers was computed using the Drude model with experimental material parameters [13], no absorption in the QCL active zone was taken into account. The wafer was processed into (16-20)-µm-wide ridges and deep mesa devices using standard optical photolithography and wet chemical etching. The substrate was then thinned down to 150 µm and cleaved into (1-3.6)-mm-long bars that were soldered with In onto copper heatsinks epi-side up. The devices were contacted to the metallized back side of the substrate and to the top of the n+-InAs cladding layer. The QCLs were tested in pulsed mode (333 ns/12 kHz) on the bars in a temperature stabilized probe station at 300K or in a flow LN_2 cryostat using wire bonding of selected devices. In both configurations, emission spectra were recorded with a Bruker V70 infrared Fourier transform

spectrometer (FTIR) equipped with a pyroelectric detector. An additional 30 Hz current modulation was applied for pulsed measurements of light-current curves with the slow FTIR detector. The reference lasers were fabricated and tested in the same way.

3. Results and discussion

Figure 4 displays the voltage-current (V-I) and light-current characteristics of 3.6-mm-long QCLs grown on Ge (EQ1092) in comparison with reference devices grown on a native InAs substrate (EQ1091). The QCLs grown on Ge exhibit threshold current densities J_{th} of 0.8-0.85 kA/cm^2 in pulsed mode at room temperature (RT) compared to 0.71-0.73 kA/cm^2 for the reference devices of the same length. It is worth noting only a small additional voltage drop in the V-I characteristics introduced by the use of a Ge substrate, which indicates a good quality of electrical contacts and low resistance of the interface region between the QCL structure and the substrate. The large density of in-plane misfit dislocations is known to create a carrier density as high as 10^{20} cm^{-3} in GaSb [14] that renders the GaSb/Ge interface highly conductive. Due to the specific type-III band alignment the p-GaSb/n-InAs heterojunction behaves as an ohmic contact [15].

The initial slope efficiency of these lasers is 110-120 and 120-135 mW/A, for EQ1092 and EQ1091 QCLs, respectively, with an optical power reaching 80 mW for the best

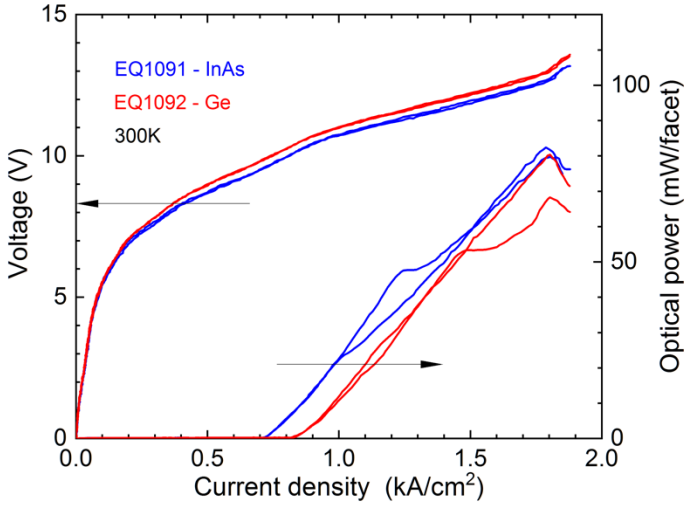

Fig.4. Voltage-current (left scale) and light-current (right scale) characteristics of two 3.6-mm-long lasers from both studied wafers. The ridge width is 18 and 19 μm for the lasers EQ1091 and EQ1092, respectively.

devices. The temperature dependence of the threshold current is very similar for the devices fabricated from both studied wafers (Fig.5) with a characteristic temperature T_0 of this exponential dependence close to 160 K. Emission spectra of the QCL presented in the insets in Fig.5 are centered at 13.8-14.0 μm, slightly below 14.2 μm expected from the simulations.

Figure 6 shows the threshold current densities of the studied QCLs fabricated from both wafers plotted as a function of reciprocal cavity length. This data can be analyzed using the general QCL threshold condition [16]:

$$J_{th} = J_{tr} + \frac{(\alpha_w + \alpha_m)}{\Gamma g} = J_{tr} + \frac{\alpha_w}{\Gamma g} - \frac{\ln(R)}{\Gamma g}\frac{1}{L}$$

where J_{tr} is the transparency current, α_m is the mirror loss depending on the laser length L, R = 0.29 the facet reflectivity calculated using the Fresnel formula for the given dielectric waveguide and g is the differential gain.

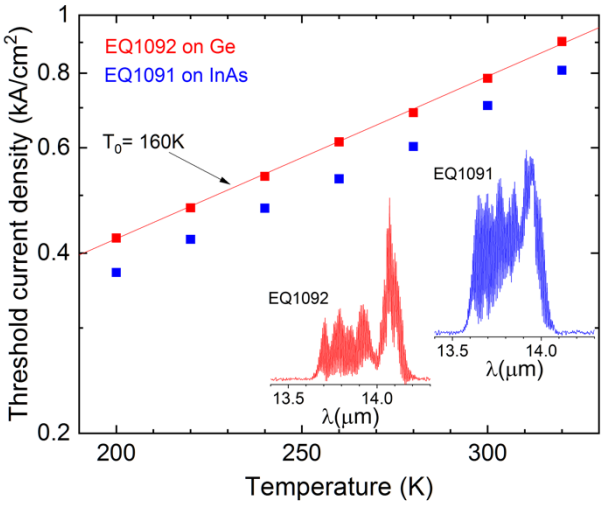

Fig.5. Threshold current density of the 3.6-mm-long QCLs as a function of temperature. The insets show RT emission spectra measured at RT at about 1.5 kA/cm^2.

The linear fits of the data in Fig.6 are parallel for both QCLs grown on Ge and the reference devices and indicate the same differential gain of 22 cm/kA that corresponds to the material gain of 44 cm/kA considering the overlap of the optical mode with the gain region. The threshold current densities of the lasers grown on Ge are higher by about 15% compared with the devices grown on the native substrate. It is interesting to note that this difference is nearly constant for devices of different lengths and does not change with temperature (Fig.4).

As can be seen from the data shown in Fig.6, the transparency current is the main component of the threshold in the reference QCLs, whereas the waveguide loss α_w = 3.6 cm^{-1} is responsible for about 25% of the threshold current in long lasers. The transparency current includes a current associated with electrons bypassing the lasing transition in the QCL active region and also the current leakage over the ridge edges related to the device fabrication. However, the principal element of the transparency current is the thermal backfilling of the lower laser transition level, which requires an additional current J_{bf} to be injected to compensate the resulting decrease in the population inversion [17]. The impact of thermal backfilling on device performance is governed by the QCL design, namely, by the width of the injector miniband Δ_{inj}, and the doping level N_s. Comparison of the low-bias parts of the very similar voltage-current characteristics presented in Fig.4 clearly shows that there is no current related to additional leakage of any origin in the QCLs grown on Ge. The small extra voltage at higher currents can be, in principle, explained by a larger Δ_{inj}, and/or lower N_s in the EQ1092 lasers. However, both factors should reduce the thermal backfilling and thus J_{tr}, which is evidently not the case. It is more reasonable to attribute the observed shift of the data for the EQ1092 lasers to an additional loss α_d = 2.6 cm^{-1} in the laser waveguide (Fig.6), which, in turn, can be due to the light scattering on defects related to threading dislocations (Figs.2,3). This conclusion agrees with previously reported results on InAs-based QCLs grown on an on-axis silicon substrate [10]. Those lasers had threshold current densities 22% higher than the devices grown on the native substrate. This difference did not change much with temperature demonstrating

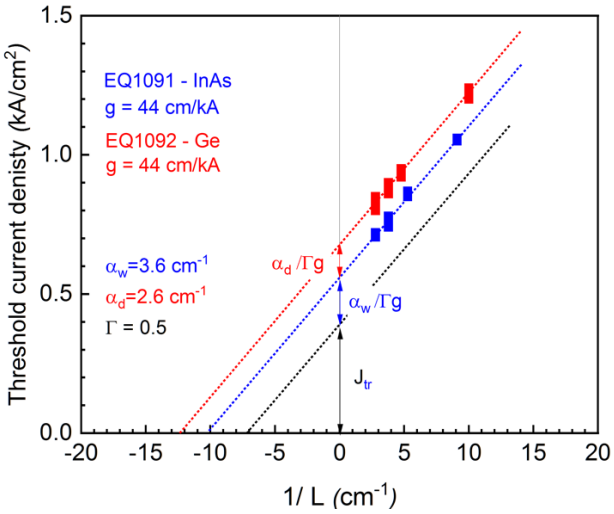

Fig.6. Threshold current density of the studied QCLs as a function of the reciprocal cavity length. At least five devices were measured at each length for both wafers.

the same T_0 value around room temperature. The observed increase in J_{th} was explained by higher optical losses because of additional absorption on crystal imperfections. In this work, we succeeded to quantify this effect by careful characterizations of lasers of different length. The weaker J_{th} degradation of 15% reflects a lower density of threading dislocations originating from the smaller lattice mismatch between the QCL material and the Ge substrate and is confirmed by the TEM observations.

One can compare these results with those of mature InP QCLs that exhibit low threshold current densities when grown on their native substrate [18] but higher densities when grown on silicon [19]. Interestingly, their properties degrade drastically as well even when heterogeneously integrated onto Si- or Ge-based platforms. Notably, their threshold current density increases in the 1.5 – 3 kA/cm^2 range, and their maximum operating temperature decreases down to 30 – 60 °C [20-22]. This is in marked contrast to the results reported here and in previous publications that show similar performance for InAs/AlSb QCLs epitaxied on their native InAs substrate, on Ge (this work), or on Si substrates [10].

4. Conclusions

In conclusion, we demonstrated InAs-based QCLs operating near 14 µm with a pulsed threshold current density as low as 0.8-0.85 kA/cm^2 in 3.6-mm-long lasers at room temperature. This value is just 15 % higher than that of the reference devices grown on a native InAs substrate. We attribute this increase in threshold current density to an additional optical loss α_d = 2.6 cm^{-1} in the laser waveguide due to light scattering on threading misfit dislocations. The high performance of the studied QCLs confirm their suitability for monolithic integration on Si/Ge mid-IR photonic circuits.

Funding. Part of this work was supported by the French Program "Investments for the Future" (Equipex EXTRA, ANR-11-EQPX-0016), the French ANR (LightUp, ANR-19-CE24-0002) and the H2020 program of the European Union (OPTAPHI, GA 860808).

Disclosures. The authors declare no conflict of interest.

Data availability. Data underlying the results presented in this article are not publicly available at this time, but may be obtained from the authors upon reasonable request.

References

1. A. Gutierrez-Arroyo, et al, "Optical characterization at 7.7 μm of an integrated platform based on chalcogenide waveguides for sensing applications in the mid-infrared," Opt. Express 24(20), 23109 (2016).
2. H. Nguyen-Van, A.N. Baranov, Z. Loghmari, L. Cerutti, J.-B. Rodriguez, J. Tournet, G. Narcy, G. Boissier, G. Patriarche, M. Bahriz, E. Tournié, and R. Teissier, "Quantum cascade lasers grown on silicon, " Sci Rep 8, 7206 (2018).
3. L. Cerutti, D. A. Díaz Thomas, J-B. Rodriguez, M. Rio Calvo, G. Patriarche, A. N. Baranov, E. Tournié," Quantum well interband semiconductor lasers highly tolerant to dislocations," Optica 8(11), 1397 (2021).
4. H. Lin, et al, "Mid-infrared integrated photonics on silicon: a perspective," Nanophotonics 7(2), 85 (2017).
5. R. Soref, "Mid-infrared photonics in silicon and germanium," Nature Photonics 4, 495 (2010).
6. N. Hon, et al, "The third-order nonlinear optical coefficients of Si, Ge, and Si1-xGex in the midwave and longwave infrared," J. Appl. Phys. 110, 11301 (2011).
7. D. Marris-Morini, et al, "Germanium-based integrated photonics from near- to mid-infrared applications," Nanophotonics, 7(11), 1781–1793 (2018).
8. H. Liu, T. Wang, Q. Jiang, R. Hogg, F. Tutu, F. Pozzi, and A. Seeds, "Long-wavelength InAs/GaAs quantum-dot laser diode monolithically grown on Ge substrate," Nature Photonics 5, 416–419 (2011).
9. H. Kroemer, "Polar-on-nonpolar epitaxy," J. Cryst. Growth 81, 192-204 (1987).
10. Z. Loghmari, J.-B. Rodriguez, A.N. Baranov, M. Rio-Calvo, L. Cerutti, A. Meguekam, M. Bahriz, R. Teissier, E. Tournié, "InAs-based quantum cascade lasers grown on on-axis (001) silicon substrate," APL Photonics 5 041302 (2020).
11. R. Go, H. Krysiak, M. Fetters, P. Figueiredo, M. Suttinger, X. M. Fang, A. Eisen- bach, J. M. Fastenau, D. Lubyshev, A. W. K. Liu, N. G. Huy, A. O. Morgan, S. A. Edwards, M. J. Furlong, and A. Lyakh, "InP-based quantum cascade lasers monolithically integrated onto silicon," Opt. Express 26, 22389 (2018).
12. M. Rio Calvo, J-B. Rodriguez, C. Cornet, L. Cerutti, M. Ramonda, A. Trampert, G. Patriarche, É. Tournié, "Crystal phase control during epitaxial hybridization of III-V Semiconductors with silicon," Adv. Electron. Mater. 8, 2100777 (2022).
13. A.N. Baranov and R. Teissier, "Quantum cascade lasers in the InAs/AlSb material system," IEEE J. Selected Topics in quantum electronics 21 (6) 1200612 (2015).
14. M. Mehta, G. Balakrishnan, S. Huang, A. Khoshakhlagh, A. Jallipalli, P. Patel, M. N. Kutty, L. R. Dawson and D. L. Huffaker," GaSb quantum-well-based "buffer-free" vertical light emitting diode monolithically embedded within a GaAs cavity incorporating interfacial misfit arrays," Appl. Phys. Lett. 89, 211110 (2006).
15. O. Diera, M. Sterkel, M. Grau, C. Lin, C. Lauer, and M-C. Amann," Tunnel junctions for ohmic intra-device contacts on GaSb-substrates," Appl. Phys. Lett. 85, 2388 (2004).
16. S. Slivken, A. Evans, W. Zhang, and M. Razeghi, "High-power, continuous-operation intersubband laser for wavelengths greater than 10 μm, " Appl. Pys. Lett. 90, 151115 (2007).
17. D. Botez, J. C. Shin, L. J. Mawst, I. Vurgaftman, J. R. Meyer and S. Kumar, "Suppression of carrier leakage in 4.8 μm - emitting quantum cascade lasers," Proc. of SPIE 7616, 76160N (2010).
18. F. Wang, S. Slivken, D. H. Wu, and M. Razeghi," Room temperature quantum cascade laser with ∼31% wall-plug efficiency," AIP Adv. 10, 075012 (2020).
19. R. Go, H. Krysiak, M. Fetters, P. Figueiredo, M. Suttinger, X. M. Fang, A. Eisenbach, J. M. Fastenau, D. Lubyshev, A. W. K. Liu, N. G. Huy, A. O. Morgan, S. A. Edwards, M. J. Furlong, and A. Lyakh, "InP-based quantum cascade lasers monolithically integrated onto silicon," Opt. Express 26(17), 22389-22393 (2018).
20. A. Spott, J. Peters, M.I. Davenport, E.J. Stanton, C.D. Merritt, W.W. Bewley, I. Vurgaftman, C.S. Kim, J.R. Meyer, K. Kirch, L.J. Mawst, D. Botez, J.E. Bowers, "Quantum cascade laser on silicon," Optica 3, 545 – 551 (2016).
21. A.Malik, A. Spott, E.J. Stanton, J.D. Peters, J.D. Kirch, L.J. Mawst, D. Botez, J.R. Meyer, and J. E. Bowers," Integration of Mid-Infrared Light Sources on Silicon-Based Waveguide Platforms in 3.5–4.7 μm Wavelength Range," IEEE J. Selected Topics in quantum electronics 25 (6) 1502809 (2019).
22. E.J. Stanton, A. Spott, J. Peters, M.L. Davenport, A. Malik, N. Volet, J. Liu, C.D. Merritt, I. Vurgaftman, C.S. Kim, J.R. Meyer and J.E. Bowers, "Multi-Spectral Quantum Cascade Lasers on Silicon With Integrated Multiplexers," Photonics 6, 6 (2019).